Clim Dyn
DOI 10.1007/s00382-012-1425-x

# A possible new mechanism for northward propagation of boreal summer intraseasonal oscillations based on TRMM and MERRA reanalysis

**S. Abhik · M. Halder · P. Mukhopadhyay · X. Jiang · B. N. Goswami**

Received: 3 January 2012 / Accepted: 13 June 2012


**Abstract** Boreal summer intraseasonal oscillations (BSISOs) manifest in the active and break spells and act as the primary building block of the Indian summer monsoon. Although recent research has evolved a basic framework for understanding the scale selection and northward propagation of the BSISO, the role of different hydrometeors in modulating these processes remains poorly explored. In this study, TRMM-2A12 retrievals and Modern Era Retrospective-analysis for Research and Applications reanalysis data are examined to establish relationship between cloud hydrometeors and other atmospheric dynamical parameters with the northward propagation of the BSISOs. The study reveals that the cloud liquid water leads the deep convection during the northward propagation of BSISOs in the lower troposphere, while the cloud ice slightly lags the convection. This distribution indicates the occurrence of a possible mechanism of the lower level moistening through the large scale moisture advection in lower atmosphere and boundary layer (PBL) convergence, followed by triggering of the deep convection. The analyses of moisture advection and the dynamical fields with respect to the convection center show that low level moistening is a manifestation of the barotropic vorticity and PBL convergence of moisture anomaly north of the convection center. A new internal dynamical-thermodynamical mechanism is unraveled to understand the reason behind the middle tropospheric heating maximum and its role on the northward propagation. It is shown that the enhanced moisture perturbation in lower levels together with the heat transport by the sub-grid scale eddies within the PBL induces lower level instability required to precondition the lower atmosphere for triggering the deep convection. Vigorous upward motion inside the deep convection uplifts the liquid hydrometeors to upper levels and the formation of precipitable ice leads to the heating maxima in the middle troposphere. To check the robustness of the proposed hypothesis, similar analysis is performed for the weak northward propagating BSISO cases.

**Keywords** Boreal summer intraseasonal oscillation · Cloud hydrometeors · Diabatic heating · TRMM · MERRA

## 1 Introduction

Intraseasonal oscillations (ISOs) are the dominant mode of variability over global tropics (Lau and Waliser 2005; Zhang 2005). An equatorially trapped eastward propagating convection anomaly during boreal winter, popularly known as Madden-Julian Oscillation (MJO; Madden and Julian 1971, 1994) and a northward propagating convection anomaly during boreal summer (Sikka and Gadgil 1980; Cadet 1986; Lawrence and Webster 2002) are the key features of the tropical ISOs. These quasi-periodic oscillations manifest in the form of active and break cycles of Indian summer monsoon (ISM; Goswami 2005) and are considered as the major building blocks of the ISM rainfall. The boreal summer ISO (BSISO) represents a signal with amplitude as large as the annual cycle and much larger than the inter-annual variability of the seasonal mean (Waliser 2006; Goswami et al. 2011). The large amplitude and its inherent quasi-periodic nature lead to a potential

S. Abhik · M. Halder · P. Mukhopadhyay (✉) · B. N. Goswami
Indian Institute of Tropical Meteorology, Dr. Homi Bhabha Road, Pashan, Pune 411008, India
e-mail: parthasarathi64@gmail.com; mpartha@tropmet.res.in

X. Jiang
Joint Institute for Regional Earth System Science and Engineering, University of California, Los Angeles, CA, USA

Published online: 04 July 2012

predictability of 25–30 days for the BSISO. As a result, extended range prediction of BSISO has received a considerable attention (Goswami and Xavier 2003; Webster and Hoyos 2004; Chattopadhyay et al. 2008).

Many important contributions have been made towards understanding the underlying mechanisms associated with the poleward propagation of BSISO. Webster (1983) proposed that the poleward gradient of sensible heat flux from planetary boundary layer (PBL) is responsible for the northward propagation of the band of cloudiness associated with the tropical convergence zone (TCZ). Goswami and Shukla (1984) also indicated that the convection-thermal relaxation process may be responsible for the northward propagation of the BSISOs. Subsequently, other studies such as Wang and Xie (1997); Lawrence and Webster (2002) attempted to explain the northward propagation resulting from unstable Rossby wave response from eastward propagating equatorial wave packets. Jiang et al. (2004) proposed that a combination of vertical wind-shear mechanism and moisture convection feedback mechanism is essential for the northward propagation of the convection. They showed that the northward shift of enhanced lower level moisture convergence along with a positive equivalent barotropic vorticity perturbation help in preconditioning the lower atmosphere for the northward propagation of BSISO convection. Additionally, the role of atmosphere–ocean coupling for the northward propagation of the BSISO has also been emphasized (Fu et al. 2003; Yang et al. 2008).

Although significant progress has been made towards understanding the northward propagating BSISOs, the interaction between small-scale convective processes and large-scale circulation in the genesis and evolution of the BSISOs, remains poorly explored. The skill of the current weather/climate models remains low in simulating the spatio-temporal characteristics and the variability of the BSISOs (Lin et al. 2008). Some studies (Fu et al. 2006) indicate that the lack of understanding and inadequate representation of the moist processes is main sources of uncertainty in the weather and climate models. The role of different cloud regimes in influencing the eastward propagating MJOs has received much attention, in many recent studies (e.g. Kikuchi and Takayabu 2004; Jakob and Tselioudis 2003; Rossow et al. 2005; Chen and Del Genio 2009; Tromeur and Rossow 2010) as compared to their role in the northward propagation of the BSISO. The results of these studies support the importance of the cumulus congestus cloud in the preconditioning of the deep convection associated with MJO. Further, it is also evident that the coupling between shallow heating from the congestus clouds and circulation in PBL are responsible for the destabilization required for the onset of MJO deep convection.

However, a similar understanding of the cloud processes associated with the northward propagation of BSISO is yet to be established. Recent studies (Xavier el al 2007; Jiang et al. 2011b, Wong et al. 2011) have showed that the vertical tropospheric diabatic heating profile plays an important role on the northward (eastward) propagation of boreal summer (winter) ISO. Based on CloudSat observation and reanalysis dataset, Jiang et al. (2011a) identified that shallow clouds in the lower troposphere lead deep convection and play an important role in shifting the deep convection northward. However, there is still a major need to understand the dynamical mechanism that controls the distribution of different cloud hydrometeors on the evolution of BSISOs. Additionally, the mechanism through which the vertical distribution of diabatic heating influences the northward propagating BSISOs also needs to be explored. Therefore, this study aims to improve our understanding of the processes responsible for the vertical distribution of heating, and through it aims to provide some new insight towards regulation of the northward propagation of BSISO.

In view of the above scientific need, we attempt to answer the following science questions: what is the role of different cloud hydrometeors (e.g. cloud water, precipitable ice and cloud ice) on the northward propagation of BSISOs? Why does the vertical profile of diabatic heating ($Q_1$) show a maximum in the middle troposphere? We also attempt to highlight the space–time characteristics and the organization of the cloud hydrometeors and the vertical heating distribution during the northward propagation of BSISOs. The rest of the paper is arranged as follows: sect. 2 describes the data and methodology, followed by the results and discussion in sect. 3 and the summary of the study in sect. 4.

## 2 Data and methodology

Daily Global Precipitation Climatology Project (GPCP, version 1.1; Huffman et al. 2001) rainfall data for the period of 1998–2008 with 1° × 1° horizontal resolution is used to identify the BSISO events. It contains several microwave and infrared (IR) satellite estimates. The daily anomalies are obtained by removing the annual cycle (mean and first three harmonics) from daily precipitation data. The same methodology has been applied for calculating daily anomalies from all other datasets. Based on relatively high and homogeneous intraseasonal rainfall variability (Fig. 1), the core region of central India (73°E–85°E and 18°N–28°N) is selected to identify the BSISO events. Earlier studies have shown the existence of two prominent modes of 10–20 day and 30–60 day within 10–90 day broadband spectrum of BSISOs, where the

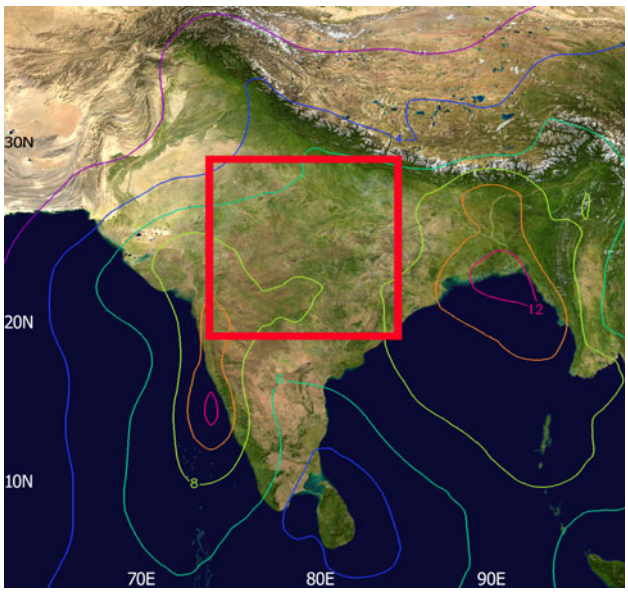


**Fig. 1** Standard deviation of 10–90 day filtered GPCP rainfall anomalies (mm day$^{-1}$) based on 1998–2008 JJAS seasons. The *red box* represents the region (73°E–85°E; 18°N–28°N) over which the precipitation index (PI) is being computed

30–60 day mode has a significantly strong northward propagating component than that of 10–20 day mode (review Goswami 2005). Power spectrum analysis of daily precipitation anomalies from GPCP over the region also supports the existence of significant power in the two frequency ranges (Figure not shown). In order to identify the BSISOs, a precipitation index (PI) is computed for each year from 1 June to 30 September using 10–90 day filtered (Duchon 1979) precipitation over the same region. The time series of the Index is normalized by its own standard deviation (3.76 mm day$^{-1}$). In order to isolate the strong BSISO cases, we consider PI value $>+1.5$ for consecutive 3 days or more (marked with filled circle in Fig. 2) and $0.4 < \text{PI} < 1.0$ for consecutive 3 days or more corresponds to the weak BSISO cases (open circles in Fig. 2). Based on the criteria, 22 strong and 17 weak BSISO cases are identified during 11 boreal summer periods. For a particular northward propagating case, the "lag 0" is identified as the day on which the PI value attains the maximum. We noted that identification of the dates corresponding to the strong and weak BSISO events are not sensitive to small changes in the area over which the 10–90 day filtered is averaged to compute the PI.

The Tropical Rainfall Measuring Mission (TRMM) 3B42 rainfall observations (Huffman et al. 2007) during 1998–2008 based on multi-satellite and rain-gauge analysis are also employed in this study. This dataset provides 3 hourly gridded precipitation estimates at 0.25° × 0.25° spatial resolutions over the global tropics (180°W–180°E, 50°S–50°N). Additionally, stratiform component of rainfall from TRMM 3G68 dataset (1998–2008) is examined. It is a combination of various TRMM products—2A12, 2A25 and 2B31 (Haddad et al. 1997a, b; Iguchi et al. 2000; Kummerow et al. 2001), available at 0.5° × 0.5° horizontal resolutions along the global tropics (40°S–40°N). This dataset include the total number of pixels, the number of rainy pixels within 0.5° × 0.5° grid, the rain rate (mm h$^{-1}$) estimates from rainy pixels and the percentage of convective rain based on 2A25 algorithm. The 3-hourly total rain rate is converted into the daily rain rate (as the frequency of observation is once a day) by multiplication of 24 and further the stratiform rain rate is computed at each grid by subtracting the convective percentage (following Chattopadhyay et al. 2009).

TRMM 2A12 hydrometeor (cloud water, cloud ice and precipitable ice) estimations (Kummerow et al. 1998, 2000; Wang et al. 2009) of 11 years (1998–2008) are primarily utilized to study the spatio-temporal distribution of different phases of hydrometeors associated with northward propagation of BSISO. This dataset is developed based on an empirical analysis technique. The algorithm assumes the cloud-model (goddard cumulus ensemble model: GCEM) generated microphysical profiles and further compute the vertical hydrometeor profiles on a pixel by pixel basis at 14 vertical levels considering the nine-channel observations of TRMM microwave imager (TMI). This orbital dataset is available in a global belt between 38°S and 38°N with 16 orbits per day. Finally, the orbital data is interpolated into gridded data having horizontal resolution of 0.25° × 0.25°.

Additionally, TRMM diabatic heating ($Q_1$) data is also utilized in this study. This is based on a "trained'' radiometer heating algorithm (Grecu and Olson 2006; Grecu et al. 2009; Jiang et al. 2011b). This dataset is a combination of TRMM precipitation radar (PR) and TMI observations. It has the horizontal resolution of 0.5° × 0.5° and is vertically interpolated into 16 pressure levels between 925 and 115 hPa from their original 29 z-levels between surface and 18 km vertical extent.

To examine the relationship between the cloud hydrometeors, diabatic heating and dynamical parameters during northward propagation of BSISO events, the Modern Era Retrospective-analysis for Research and Applications (MERRA) is utilized (Bosilovich and coauthors 2006). MERRA is a National Aeronautics and Space Administration (NASA) atmospheric reanalysis for the satellite era using a major new version of the Goddard Earth Observing System Data Assimilation System version 5 (GEOS-5). The global dataset with horizontal resolution of 1.25° × 1.25° and 42 pressure levels between 1,000 and 0.1 hPa is available from 1979 to present at the website: http://disc.sci.gsfc.nasa.gov/daac-bin/FTPSubset.pl. The daily dataset include the zonal and meridional wind components (u, v), vertical p-velocity ($\omega$), temperature, specific

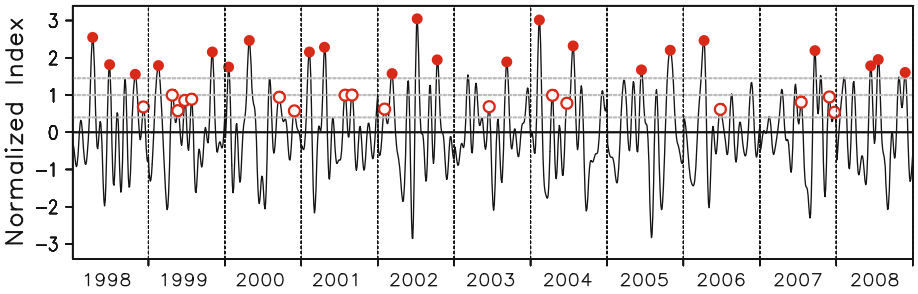


**Fig. 2** Time series of normalized PI between 1 June and 30 September (122 days) during 1998–2008 using GPCP. PI is defined as 10–90 day filtered rainfall anomaly averaged over 73°E–85°E and 18°N–28°N. The time series is normalized by its own S.D. (3.76 mm day$^{-1}$). *Filled* (*open*) *red circles* indicate peaks of strong (weak) BSISO phases

humidity and relative humidity. Further, the vertical profile of vorticity and divergence are computed using u and v-wind components. In addition to that, total diabatic heating ($Q_1$) is also used from MERRA reanalysis.

The total diabatic heating is a combination of heating from radiative, moist and turbulent processes and can be written as:

$$Q_1 \approx Q_R + L(c-e) - \frac{\partial}{\partial p}\left(\omega' \theta'\right) \quad (1)$$

MERRA reanalysis also provides the heating due to radiative ($Q_R$) and moist processes (second term on the RHS of Eq. 1). So, by subtracting the combination of the heating due to the radiative and moist processes from the total diabatic heating should provide the vertical transport of the heat by the sub-grid scale eddies (third term in the RHS of Eq. 1).

$$-\frac{\partial}{\partial p}\omega' \theta' = Q_1 - Q_R - L(c-e) \quad (2)$$

## 3 Results and discussions

As mentioned earlier, we classified the BSISO events broadly into two categories; strong and weak (see sect. 2). To examine the large scale organization of precipitation during strong BSISO events, we constructed the lag composite of GPCP precipitation anomalies (Fig. 3) with respect to the peak of the PI index based on 22 strong BSISO events. At "lag −12", positive rainfall anomalies develop over equatorial Indian Ocean (EIO). Further, they intensify and gradually progress northward from EIO region to the monsoon trough (MT) region by "lag 0". This situation corresponds to the active phase of the ISM. At "lag 0", negative anomalies are prominent over EIO region. Subsequently, the positive rainfall anomalies further move to the foothills of the Himalaya followed by negative rainfall anomalies covering the MT region. The suppressed convection over the MT region is associated with break condition of ISM. The lag-composite analysis shows a meridional dipole structure in rainfall anomalies over the Indian Ocean sector associated with the northward propagation of the strong BSISO events. Figure 3 also indicates that the horizontal scale of the strong BSISO cases covers large region with the meridional wavelength of about 20°. To illustrate the propagation characteristics of the BSISOs, lag-latitude plots of rainfall anomaly for strong (Fig. 4a) events averaged over 70°E–90°E are constructed. A well-organized northward propagation of positive rainfall anomaly followed by a negative rainfall anomaly from EIO up to about 25°N at the rate of about 1°day$^{-1}$ is evident for the strong BSISO events (Fig. 4a). Lag composites of rainfall anomalies based on 17 weak events indicate that they are not well organized on large scale as in the case of strong cases (figure not shown). A well-defined northward propagation is also missing during weak BSISO events (Fig. 4b). It may be noted that the strong events are associated with the lower frequency of BSISO (Fig. 4a) while the weak events are associated with the higher frequency component of BSISO (Fig. 4b). It is interesting to note that the criteria based on which the strong and weak BSISO events are identified, essentially separates the low (30–60 day mode) and high (10–20 day mode) frequency BSISOs respectively (Fig. 4). The lack of northward propagation in weak BSISO cases (Fig. 4b) is also consistent with the separation of the 10–20 day mode, which is known to have no prominent northward propagation.

### 3.1 Northward propagation of cloud hydrometeors

In order to examine the cloud regimes associated with the strong BSISO phases, the time evolution of composite pressure-latitude section of 3 day mean anomalous TRMM estimated cloud liquid water (CLW; top panel, shaded) along with TRMM 3B42 precipitation anomalies [bottom panel, red (blue) shading stands for enhanced (reduced) rainfall activity] averaged over 70°E–90°E are shown in Fig. 5. The CLW is found to be confined mainly below 400 hPa with the maxima located around 700 hPa.

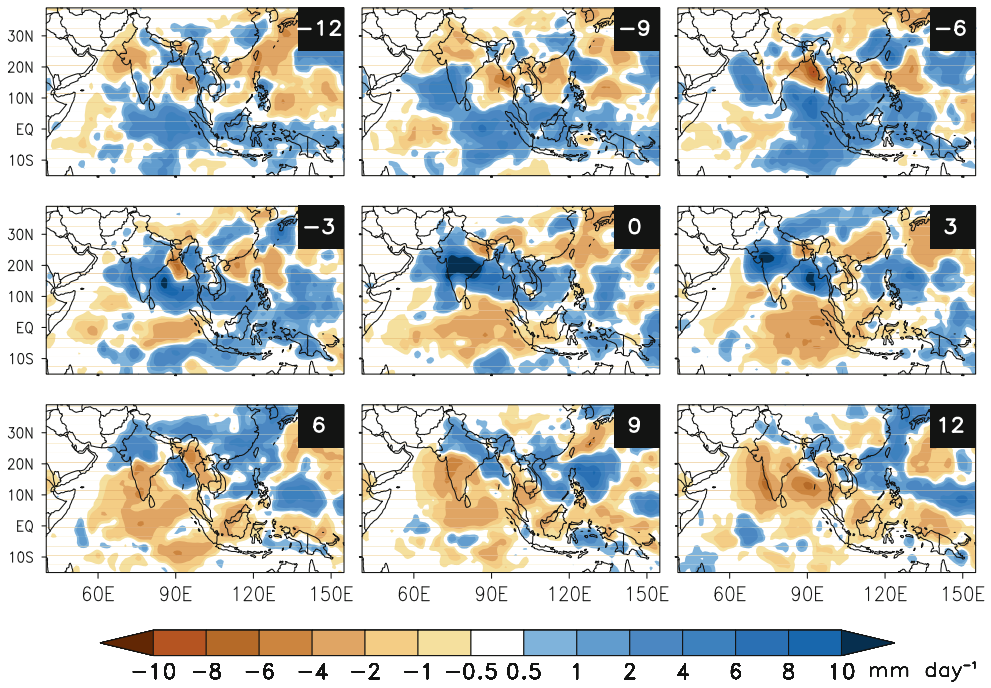


**Fig. 3** Lag-composite of GPCP precipitation anomaly (mm day$^{-1}$, *shaded*) for strong BSISO cases

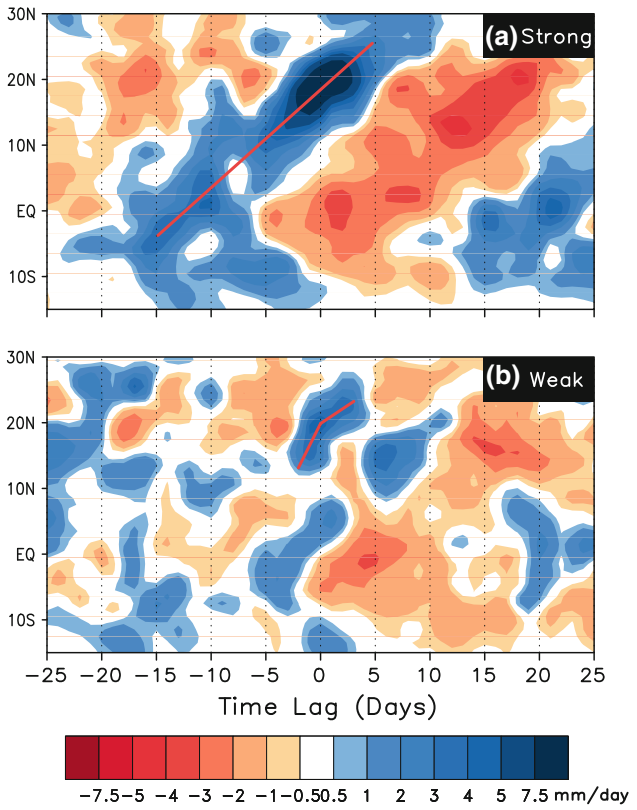


**Fig. 4** Lag-Latitude plot for GPCP precipitation anomaly (mm day$^{-1}$, *shaded*) averaged over 70°E–90°E for **a** strong and **b** weak BSISO cases. *Red solid lines* are drawn to indicate the propagation speed of the rainfall anomaly

Initially, the CLW anomalies originate from the EIO region at −12 lag and show a steady northward progression together with the anomalous rainfall. Similar to CLW, anomalous cloud ice (CI) profiles from TRMM also exhibit organized northward propagation along with the precipitation anomaly (contours in Fig. 5). The CI is confined above 400 hPa with the maximum at around 200 hPa. Precipitable ice (e.g. graupel, snow), another important mixed-phase hydrometeor which plays an important role in the latent heat release in the middle troposphere and precipitation formation, also shows a quasi-periodic propagation characteristic similar to the rainfall and other hydrometeors (figure not shown). Along with the hydrometeors, we further analyzed the TRMM derived diabatic heating ($Q_1$) profile for strong BSISO events during 1998–2007 (Fig. not shown). The heating maximum is found to be in the middle troposphere around 500 hPa. As the rainfall propagates northward from EIO region, the diabatic heating shows a steady northward migration signifying the shift of convection zone to the north.

In contrast to the organized northward propagation of the strong BSISO events, the weak BSISOs do not show such a prominent northward propagation (Fig. 4b). The evolution of cloud hydrometeors and diabatic heating anomalies associated with the weak BSISO events have rather smaller scale regional characteristics (figure not shown) and are not well organized as compared to strong northward propagating cases. Further, the weak BSISOs

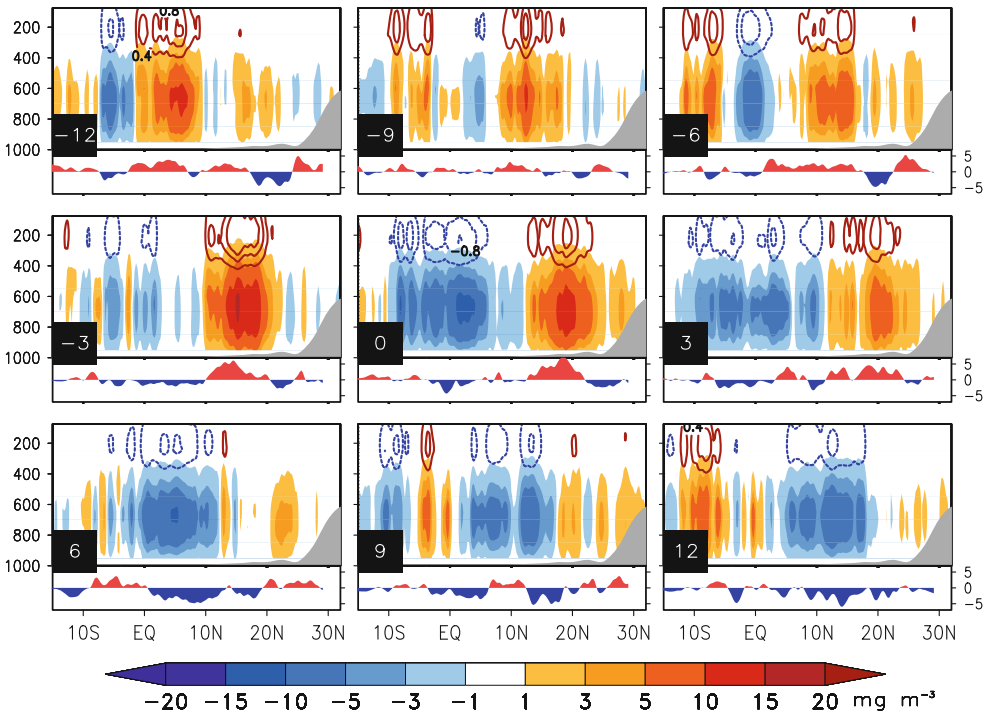


**Fig. 5** Lag composite of pressure-latitude profiles of anomalous TRMM cloud water (mg $m^{-3}$, *shaded*) and cloud ice (mg $m^{-3}$, contoured with minimum contour and contour interval of 0.4 mg $m^{-3}$) over Indian region (70°E–90°E), based on composite analysis of 22 strong BSISO events during 1998–2008. At lower part corresponding 70°E–90°E averaged rainfall (mm $day^{-1}$) from TRMM 3B42 are shown. The *red* (*blue*) shading denotes enhanced (reduced) rainfall activity. "Lag 0" represent the day on which maximum convection anomaly occurs over central India box

(10–20 day mode) are associated with westward propagation over the Indian region. Since this study primarily aims to highlight the northward propagation of the BSISOs, the westward component has not been analyzed thoroughly.

### 3.2 Dynamical response to the BSISO

Although the above analyses indicate the quasi-periodic oscillations in cloud hydrometeors, it does not reveal the cause and effect relationship among the cloud hydrometeors and rainfall. In order to explain the phases of the hydrometeors and associated dynamical parameters more clearly, we have composited the meridional-vertical structure of anomalous vorticity ($\times 10^{-6}$ $s^{-1}$, Fig. 6a), divergence $10^{-6}$ $s^{-1}$, Fig. 6b), vertical pressure–velocity (hPa $s^{-1}$, Fig. 6c) and specific humidity (g $kg^{-1}$, Fig. 6d) fields using MERRA reanalysis data with respect to the maximum convection center (MCC). It may be noted that the MCC are identified based on rainfall maxima following the methodology of Jiang et al. (2004). The positive (negative) numbers in the abscissa correspond to the distance in degrees to the north (south) direction with respect to the MCC. The analysis indicates that the vertical structure of the northward propagating strong BSISOs has a significant barotropic component together with a baroclinic component. Drbohlav and Wang (2005) suggested that baroclinic mode is important for the intensification of convection, whereas the barotropic component helps in the initiation and propagation of the convection. The vertical distribution of vorticity shows (Fig. 6a) an equivalent barotropic structure and the center of positive vorticity lies about 4° north of MCC. In contrast, a negative vorticity appears to the south of the MCC. The lower level convergence and the upper level divergence to the north of the MCC are also evident from the vertical structure of divergence field (Fig. 6b). Consistent with the divergence field, a barotropic structure of vertical pressure–velocity is found to be collocated with the MCC (Fig. 6c) at the lower levels and extending beyond the middle troposphere. These dynamical forcing particularly the barotropic vorticity and lower level convergence in PBL appear to help the lower level moisture convergence to the north of the MCC. As a consequence, the occurrence of maximum specific humidity (Fig. 6d) is observed within the lower troposphere (around 800–900 hPa). A northward shift of PBL moisture relative to the MCC associated with the northward propagating BSISO has also been noted in previous studies (e.g. Jiang et al. 2004; Fu et al. 2006). Recently, the study of Prasanna and Annamalai (2012) emphasized the importance of negative horizontal moisture advection

during the initiation of extended break spells of ISM. The positive anomalous horizontal moisture advection (Fig. 6e) tends to lead the convection by 6° at lower levels (around 900 hPa). Additionally, the anomalous horizontal moisture advection tilts southward with height and has the maxima around 700–800 hPa. As a consequence, it destabilizes the lower atmosphere ahead of the convection by enhancing the equivalent potential temperature ($\theta_e$). It is seen from Fig. 6f that the lower atmosphere to the north of the MCC is convectively unstable and the instability also tilts southward with height. The enhanced instability at the MCC is consistent with the active convection of strong BSISO. Nevertheless, it is argued that the northward shift of the lower tropospheric instability may cause the northward displacement of the convection by preconditioning the lower atmosphere to a new convectively unstable state.

In order to examine the robustness of the mechanisms mentioned above, 17 weak BSISO cases are also studied. Similar to Fig. 6 for strong BSISOs, Fig. 7 shows composite meridional-vertical profile of the dynamical parameters associated with northward propagating weak BSISO events. The vertical structure of vorticity (Fig. 7a) and divergence (Fig. 7b) show a much weaker signal as compared to the strong counterparts. The main differences are observed in the vertical velocity (Fig. 7c) and specific humidity (Fig. 7d) fields. Unlike the strong cases, the vertical velocity appears to be confined only in the lower troposphere for the weak cases and does not show a coherent ascending motion signifying strong convection at the MCC. Further, the horizontal advection of positive moisture perturbation to the north is also missing in weak BSISO cases (Fig. 7e). As a consequence, the organization of moisture is much weaker to the north of the MCC (Fig. 7d). This is also reflected in the vertical structure of $\theta_e$, indicating that the instability associated with weak northward propagating events is not well organized and has a smaller meridional scale than that of the strong BSISO cases.

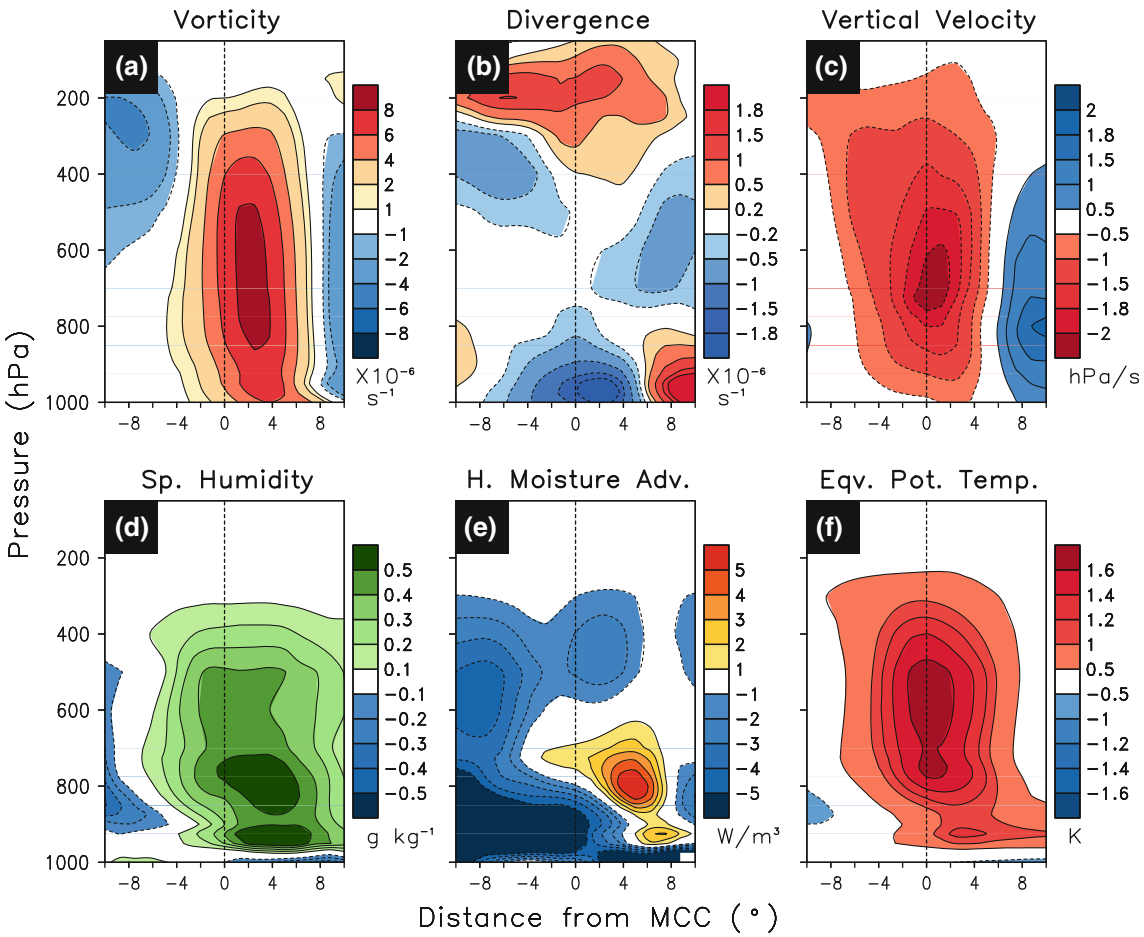


**Fig. 6** Meridional-vertical structures of the northward propagating strong BSISO events for **a** vorticity ($\times 10^{-6}$ s$^{-1}$), **b** divergence ($\times 10^{-6}$ s$^{-1}$), **c** vertical velocity (hPa s$^{-1}$), **d** specific humidity (g kg$^{-1}$), **e** horizontal moisture advection (W m$^{-3}$) and **f** equivalent potential temperature ($\theta_e$, K) from *MERRA Reanalysis*. *Horizontal axis* represents the meridional distance (degree) with respect to maximum convection center (MCC). The +ve (−ve) value means to the north (south) of MCC

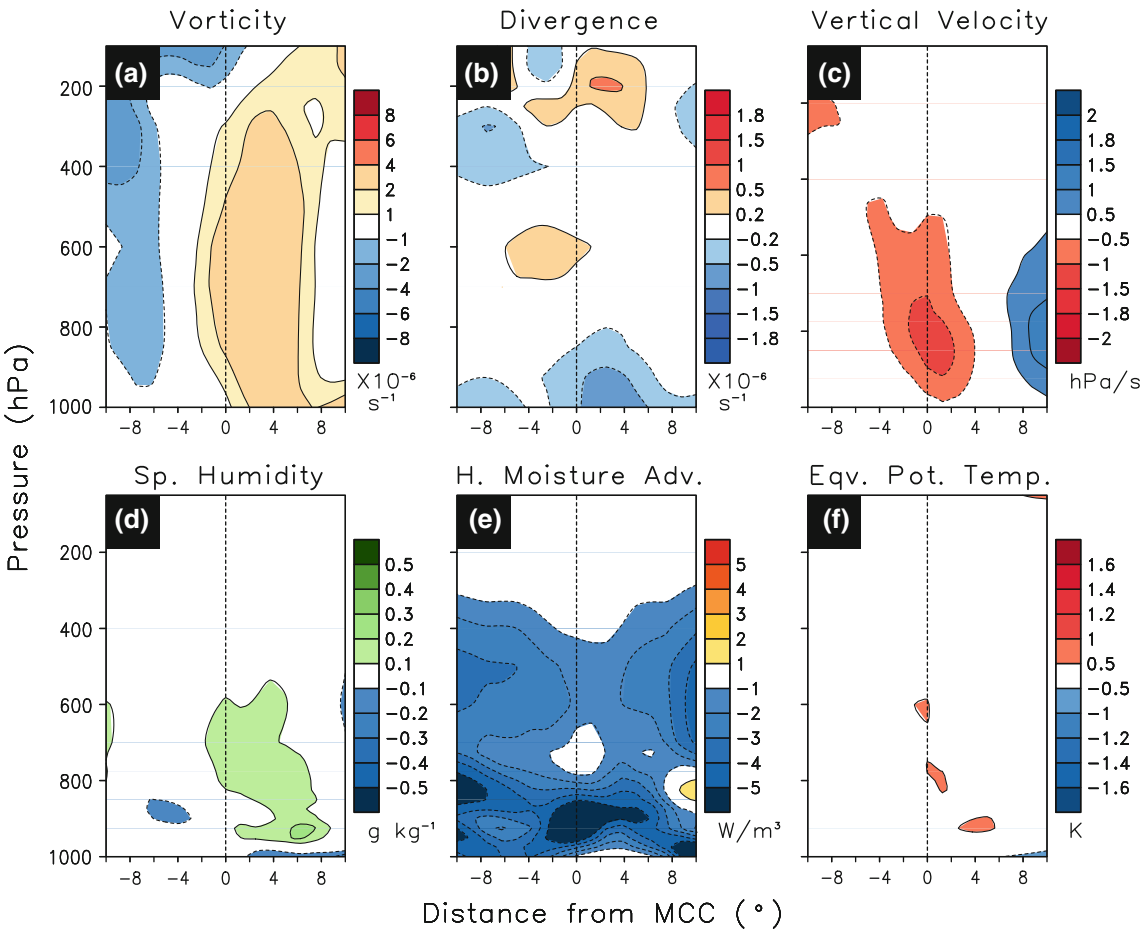


**Fig. 7** Same as Fig. 6, but for the propagation of weak BSISO phases

### 3.3 Thermodynamical response to the BSISO

The abundance of moisture to the north of the MCC leads to the formation of CLW above the condensation level (LCL). A similar composite analysis with respect to the MCC is also done using TRMM CLW (mg $m^{-3}$, Fig. 8a, shaded with contours), CI (mg $m^{-3}$, Fig. 8a, contours only). Thus, the genesis of CLW to the north of the MCC is a manifestation of the dynamical factors, such as, lower level moisture convergence, stronger vertical velocity and equivalent barotropic vorticity. Similar lower level moistening ahead of the eastward propagating MJO convection is also observed by Tian et al. (2006). The abundance of CLW at the lower troposphere (Fig. 8a, shaded with contour) appears to work as a trigger for deep convection by preconditioning the lower troposphere. It is likely that the strong updrafts inside the deep convection allow the larger water drops to grow for longer time period as they are carried relatively upward (Houze 1997). Moreover, the strong upward advection of the liquid hydrometeors well-above the freezing level gives rise to mixed-phase in the middle troposphere (Fig. 8b) and CI even in the higher levels (Fig. 8a, contours only) where generally the anvil part of the deep convective clouds are present due to lateral spreading of the ice-phase hydrometeors by the divergent air flow.

The condensation of the water vapour results in release of latent heat into the atmosphere. It can further influence the large-scale circulation through the modification of heat and moisture distribution around the convection. To further understand the heating induced circulation associated with the strong BSISOs, we have analysed the meridional-vertical profile of TRMM diabatic heating with respect to the MCC. The composite analysis shows that the heating maximum is present (Fig. 8c) in the middle troposphere (around 500 hPa) and is collocated with the MCC. However, recent studies (e.g. Zhang et al. 2010; Jiang et al. 2011b) have reported that the TRMM dataset lacks in identifying light rainfall events especially under the dominance of the shallow clouds. We, therefore, further analysed the total diabatic heating field from MERRA reanalysis (Fig. 8d). MERRA reanalysis can reproduce the diabatic heating associated with the northward propagation of BSISO, although some discrepancies have been noted

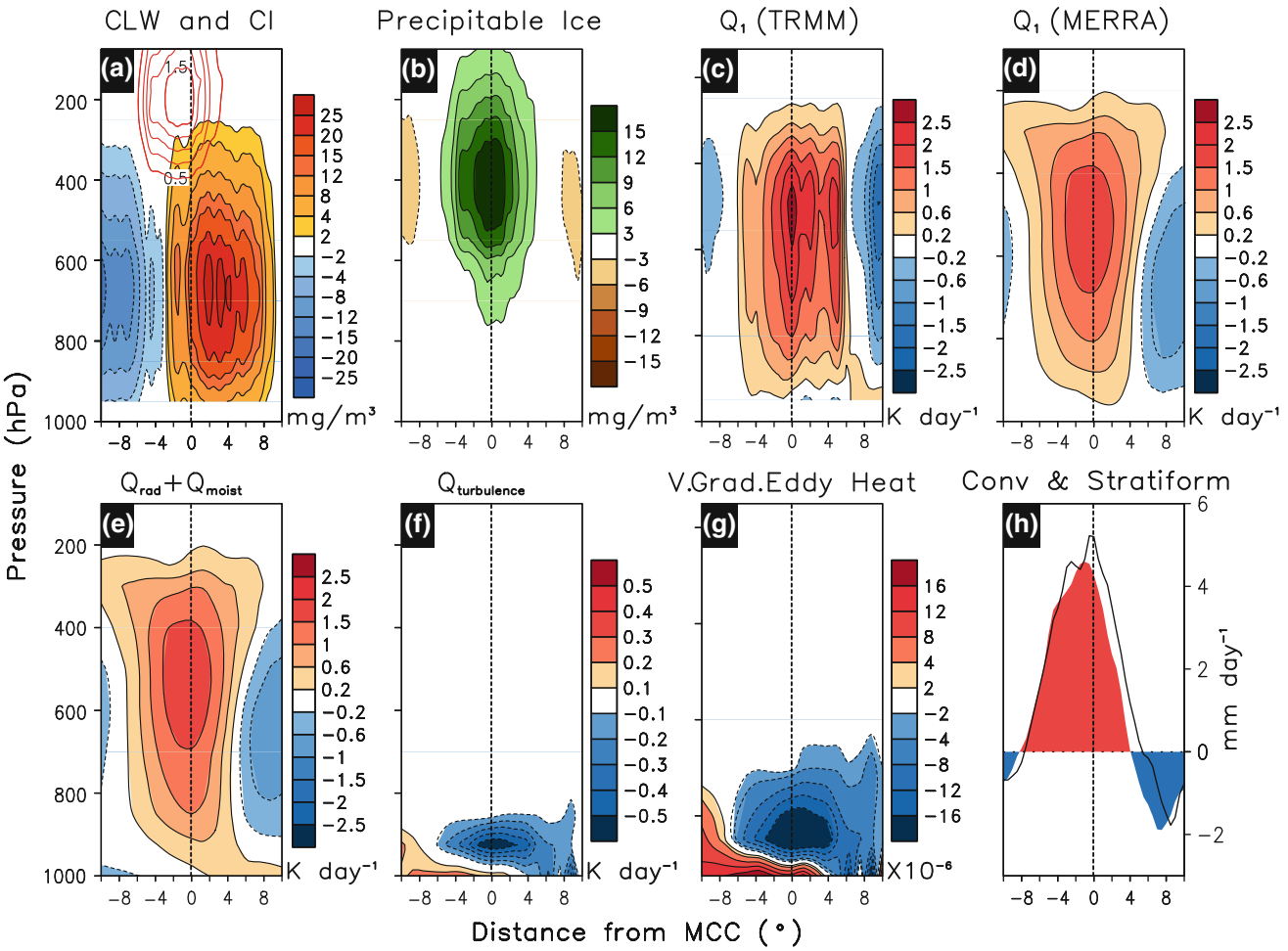


**Fig. 8** Meridional-vertical structures of the northward propagating strong BSISO events for **a** cloud water (mg $m^{-3}$, shaded with contours) and cloud ice (mg $m^{-3}$, contours only with a contour interval of 0.25 mg $m^{-3}$), **b** precipitable ice (mg $m^{-3}$), **c** diabatic heating (K $day^{-1}$) from *TRMM*, **d** diabatic heating (K $day^{-1}$), **e** diabatic heating contribution from radiative and moist processes (K $day^{-1}$), **f** vertical transport of heat by eddies (K $day^{-1}$), **g** gradient of vertical transport of eddies ($\times 10^{-6}$ K $Pa^{-1}$ $day^{-1}$) from *MERRA* reanalysis and **h** convective (mm $day^{-1}$, solid line) and stratiform rain (mm $day^{-1}$, shade) from *TRMM 3G68*. *Horizontal axis* represents the meridional distance with respect to maximum convection center (MCC). The +ve (−ve) value means to the north (south) of MCC

between the TRMM and MERRA reanalysis. It is found that MERRA underestimates the amplitude of the diabatic heating. Similar underestimation of amplitude of the diabatic heating by MERRA is also reported in a recent study by Wong et al. (2011). Further, the contribution from radiative and moist processes towards the diabatic heating as obtained from MERRA is shown in Fig. 8e. The difference between the total diabatic heating and the combination of heating from radiative and moist processes (Eq. 2) is the measure of vertical transport of heat by the sub-grid scale eddies (Fig. 8f). The sub-grid scale turbulent heat transport clearly shows the maxima at the lower troposphere, mainly within the PBL.

However, earlier observational studies have suggested that the ISM rainfall is comprised of stratiform and convective components (Chattopadhyay et al. 2009) and the stratiform rainfall is the manifestation of the anvil part of the convection or the ice-phase processes (Houze 2004). In order to study the distribution of stratiform and convective rainfall during the strong BSISO events, the TRMM 3G68 data for those two rainfall anomalies are analysed. It is observed that the maximum of the positive stratiform rainfall anomaly [red (blue) shading denotes enhanced (reduced) rainfall activity; Fig. 8h] lies about 2° south of the MCC, while the convective anomalies are more or less in phase with the MCC (solid black line in Fig. 8h). However, the negative anomalies of convective and stratiform rainfall are found on both sides of the MCC. The results suggest that the convective rainfall, which is collocated with the MCC, leads the stratiform rainfall. Interestingly, the majority of CI (Fig. 8a, contours only) also exists at the south of the MCC. Thus, it appears that the stratiform rainfall is dominated by the ice-phase processes and hence it is collocated with the CI. A similar

observation of CI to the south of the MCC is also noted by Jiang et al. (2011a).

How robust are these composites? Are the features seen in the composites common to all members of the composites? To answer this question, we calculated the standard deviation of inter member variability of all fields shown in Fig. 8 as a function of height and distance from the MCC. It is seen (figure not shown) that the inter-member variability is within 20–40 % of the mean indicating that the composite indeed indicates the underlying commonality amongst the different events.

What we have observed so far from the above analyses is that the lower troposphere is dominated by the abundant CLW to the north of the MCC, while the CI occurs slightly to the south of the MCC. The positive moisture advection to the north of the MCC may contribute to moistening and preconditioning the lower atmosphere for triggering deep convection. It is also seen from the TRMM dataset as well as from MERRA reanalyses that the diabatic heating has a maximum in the middle troposphere. However, the key question for the northward propagation of BSISO is still unanswered: how does the diabatic heating show the maxima at the middle troposphere? This question has not been addressed by any of the earlier studies related to northward propagation of BSISO. It is hypothesized that the moisture advection in the lower troposphere together with the sub-grid scale eddies in PBL may be responsible for the middle level heating maxima.

The sub-grid scale eddies transport the heat within the PBL where the turbulent mixing is strong. In order to gain more insight on the heat transport within the PBL, we have further computed the gradient of vertical eddy heat transport (Fig. 8g) following equation:

$$\tau = \frac{\partial}{\partial p}\left\{-\frac{\partial}{\partial p}(\omega'\theta')\right\} \tag{3}$$

The analysis shows that the maxima of the vertical gradient occurs around 850–900 hPa, at the top of the well-mixed PBL. The result also indicates a net upward transport of heating in the lower atmosphere and the turbulent eddies may contribute in increasing the heating induced instability within the PBL (Fig. 6f). The lower level instability ahead of the MCC would further induce the lower level convergence and strong upward motion in lower atmosphere. As a consequence, the lower level moisture would get transported upward, resulting low level clouds with abundance of CLW north of the MCC. This may eventually contribute in preconditioning the atmosphere to trigger the deep convection. Finally, the generation of precipitable ice inside the deep convective cloud as discussed earlier, would release latent heat in the middle atmosphere. The processes associated with the heat released in the middle troposphere are schematically shown in Fig. 9a. Furthermore, the mid-tropospheric heating would enhance the instability ahead of the convection and that would cause the northward displacement of the convection by preconditioning the lower atmosphere to a new convectively unstable state (Fig. 9a, b, c).

To Show the associated vertical structure of the thermodynamical parameters and the cloud hydrometeors, a similar composited meridional-vertical profile (as in Fig. 8 for strong BSISO) of the northward propagating weak BSISO events are also derived (Fig. 10). The CLW and CI (Fig. 10a) are present with significantly lesser proportion as compared to those for the strong BSISO events. The proportion of precipitable ice (Fig. 10b) is also found to be substantially less and like the strong cases it mostly occurs to the south of the MCC. The positive moisture advection, as in case of the strong BSISO events, is completely missing for the weak BSISO cases. The diabatic heating from TRMM estimate (Fig. 10c) shows a weak heating maximum in the middle troposphere. The diabatic heating profile as derived from MERRA reanalyses (Fig. 10d) and the combination heating from radiative and moist processes in MERRA reanalysis (Fig. 10e) also show weak maxima to the north of the MCC. The corresponding amount of the stratiform rainfall (Fig. 10h) also appears to be significantly small and that is consistent with the lesser proportion of CI. Since the large-scale organization of the convection is missing for weak BSISO cases, the convective rainfall exhibits multiple secondary convective regions on both sides of the MCC. This result indicates the regional characteristics of the weak BSISO events. The coherent vertical eddy heat transport, as seen for strong events, is also absent (Fig. 10f) and the gradient of eddy heat transport (Fig. 10g) shows an unusual vertical distribution with weak convergence ahead of the MCC. The analysis suggests the importance of the vertical heat transport by the sub-grid scale eddies in the lower atmosphere. It establishes the fact that such heat transport by the sub-grid scale eddies must occur during the northward propagation of the BSISO.

Therefore, it is evident from the above analyses that the sub-grid scale eddies play an important role in organizing the instability ahead of the convection during the northward propagation of the BSISO. The eddy heat transport within the PBL together with the lower-level convergence induced strong upward motion is responsible for the diabatic heating distribution in the troposphere during the northward propagation of the strong BSISO. In contrast, the contribution from both the eddy heat transport and the vertical velocity are significantly less for the weak BSISO. This supports our proposed hypothesis.

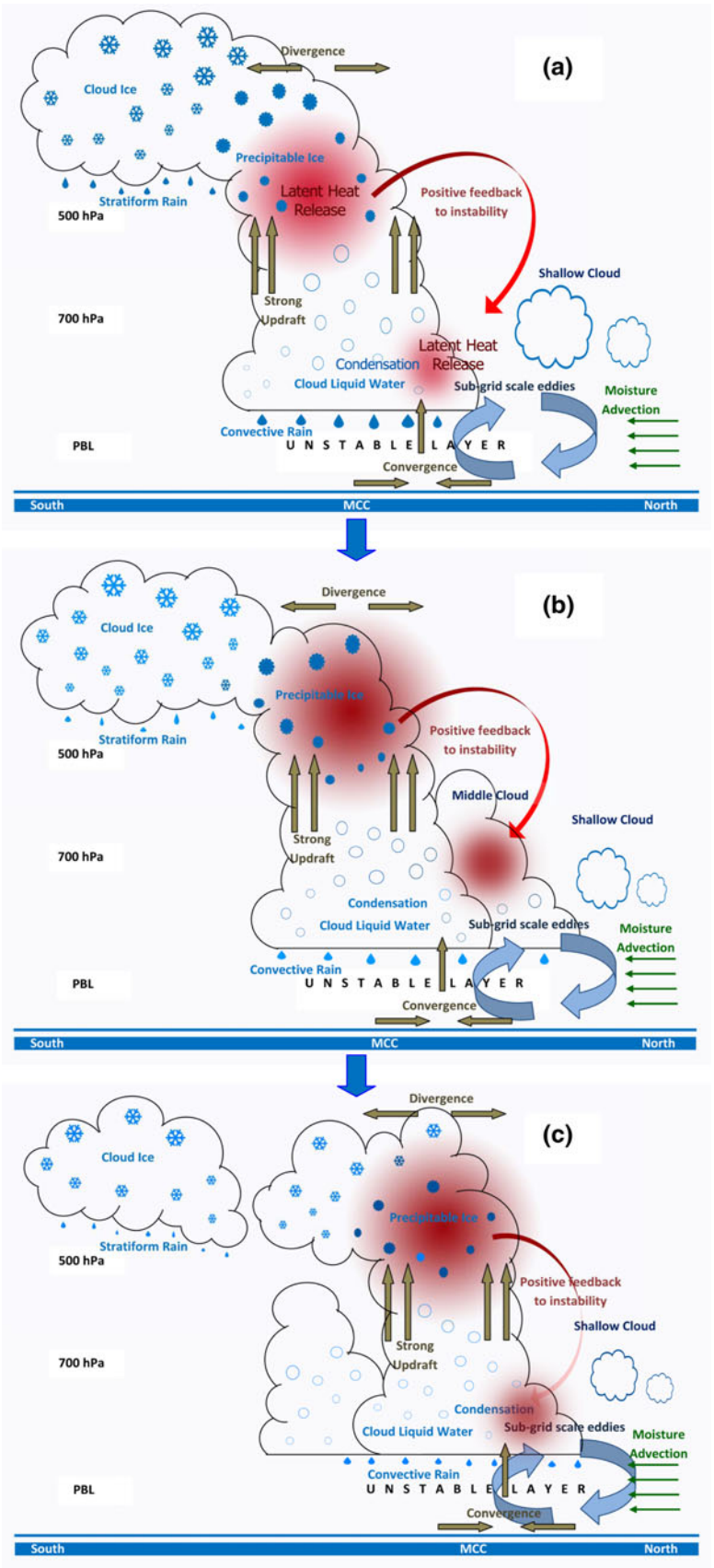


**Fig. 9** Schematic diagram (**a**, **b**, **c**) for the cloud processes associated with the northward propagation of the BSISOs (not in scale). The proposed hypothesis on the mid-tropospheric heating maxima is shown in (**a**)

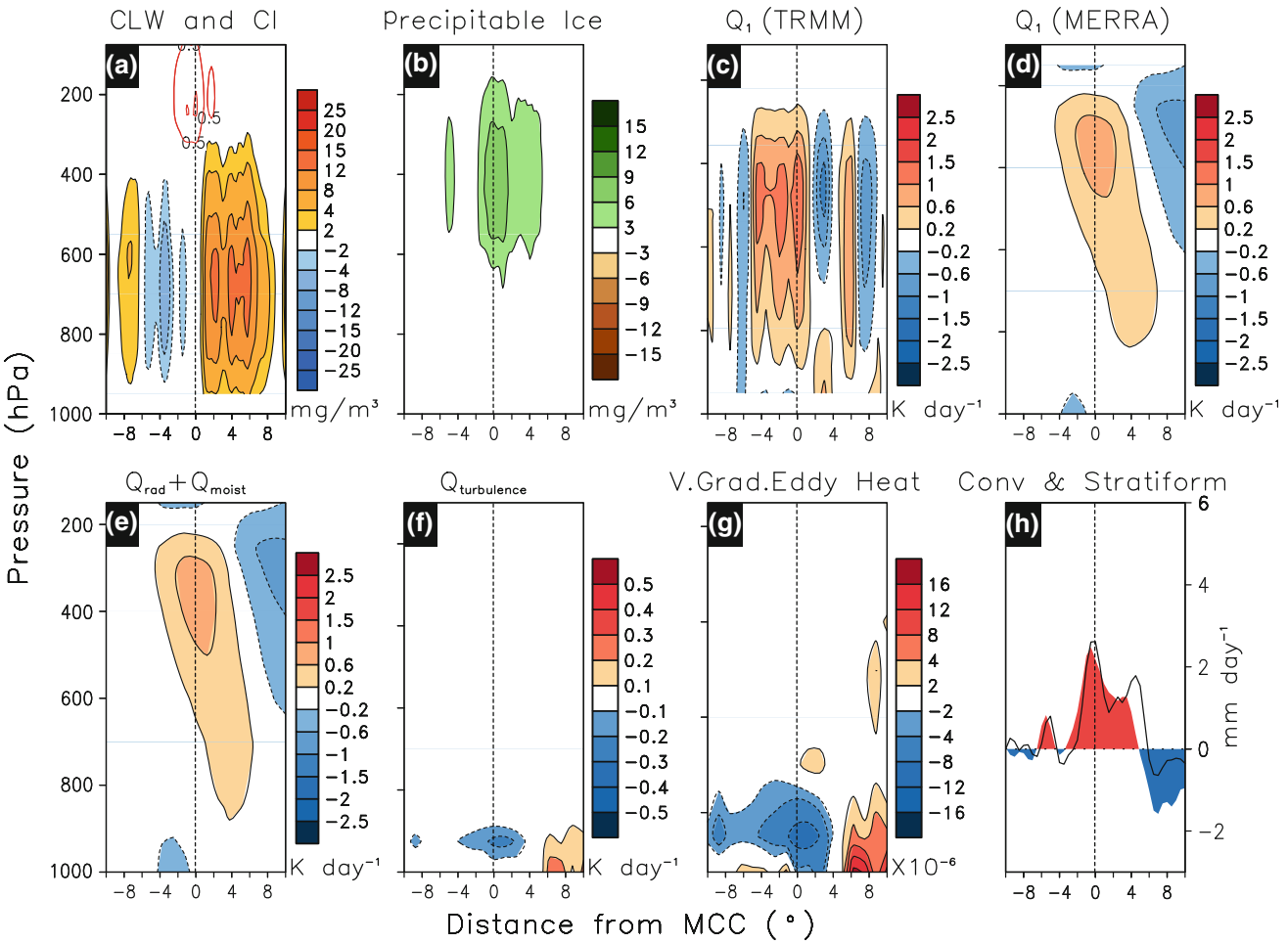


**Fig. 10** Same as Fig. 8, but for propagation of the weak BSISO Phases

## 4 Summary

The northward propagation of BSISO is an important component of the tropical climate system and the seasonal variability of the ISM rainfall depends on the spatio-temporal evolution of the BSISOs. Therefore, understanding the evolutions of cloud hydrometeors during the BSISO events will have direct impact on our capability of representing these processes in numerical models. Keeping this in view, the study addresses the role of cloud hydrometeors and associated dynamical parameters on northward propagation of BSISO using 11 years (1998–2008) TRMM data and MERRA reanalyses. Our analyses reveals that during the strong BSISO events, the hydrometeors such as CLW, precipitable ice and CI show a steady northward progression from EIO to about 25°N. Earlier diagnostic studies on the northward propagation of BSISO suggested that an equivalent barotropic vorticity and positive anomalous moisture persist to the north of the MCC. An anomalous convergence of moisture with a maximum in the lower troposphere also tends to lead the convection by a few degrees. The moisture convergence north of the MCC plays a significant role in moistening the lower atmosphere ahead of the MCC. The unstable and moist lower atmosphere preconditions the environment in triggering the deep convection and simultaneously contributes in the generation of abundant CLW through condensation ahead of the MCC. In this study, we have proposed a new mechanism for generating the heating distribution in the troposphere during the northward propagation of BSISO. The lower level moisture advection and the sub-grid scale eddies may be responsible for the generation of the instability in the lower troposphere and the lower level instability helps in triggering the deep convection. Further, the strong updraft motion inside the deep convection causes net upward displacement of the liquid hydrometeors. The updraft of the liquid hydrometeors eventually produces the precipitable ice in the middle troposphere and releases latent heat around 500 hPa. The heating at the MCC further strengthens the convection by enhancing the instability. The lower atmospheric heating-induced instability subsequently causes the enhancement of the convergence in the

lower troposphere and strengthens the lower level moisture convergence to the north of the MCC. The shifted centre of the moisture convergence will further destabilize the atmosphere to the north of the convection. As a consequence, it leads to the northward displacement of the MCC.

It is also found that the convective rainfall is in phase with the convection, whereas the stratiform rain lies to the south of the MCC and the latter is collocated with the CI. This suggests that the stratiform rain is a manifestation of the ice phase processes occurring inside the anvil part of the deep convection.

Contrary to the strong BSISO events, such large-scale organized northward propagation of the cloud hydrometeors has not been observed for the weak events, rather they show regional characteristics. The lag-latitude diagram of the precipitation anomaly also shows a dominance of higher frequency component during the weak events. These characteristics are consistent with the propagation features associated with 10–20 day mode. The diagnosis of the northward propagating weak BSISO cases unveils that asymmetric vertical structure of dynamical and thermodynamical fields are weakly organized with respect to the MCC. The positive moisture advection is completely missing for the weak BSISO cases. Consistent with the moisture advection, the instability and vertical eddy transport of heating within PBL is weak and the gradient of heat transport shows a different structure compared to the strong BSISO events. This new insight and understanding in the structure and evolution of the dynamical fields, cloud hydrometeors and the diabatic heating components is expected to help in better representation of these processes in numerical models to simulate the observed variability of the northward propagating BSISO.

**Acknowledgments** IITM, Pune is fully funded by the Ministry of Earth Sciences (MoES), Govt. of India, New Delhi. We would like to thank GSFC/DAAC, NASA for providing MERRA reanalysis, GPCP and TRMM dataset. TRMM diabatic heating dataset is kindly provided by Bill Olson. The work is a part of AS's Ph.D. dissertation, financially supported by Council of Scientific and Industrial Research (CSIR), Govt. of India. We are also thankful to the three anonymous reviewers for their constructive comments that led to improvement of the manuscript. AS would like to acknowledge Sharmila Sur for helpful discussions. The GrADS software developed by Dr. Brian Doty, COLA is also acknowledged.

## References

Bosilovich MG et al (2006) NASA's modern era retrospective-Analysis for research and applications. U S CLIVAR variations, 4. U S CLIVAR Office, Washington, DC, pp 5–8

Cadet DL (1986) Fluctuations of precipitable water over the Indian Ocean during the 1979 summer monsoon. Tellus Ser A Dyn Meteorol Oceanogr 38:170–177

Chattopadhyay R, Sahai AK, Goswami BN (2008) Objective identification of nonlinear convectively coupled phases of monsoon intraseasonal oscillation: implications for prediction. J Atmos Sci 65:1549–1569

Chattopadhyay R, Goswami BN, Sahai AK, Fraedrich K (2009) Role of stratiform rainfall in modifying the northward propagation of monsoon intra-seasonal oscillation. J Geophys Res 114:D19114. doi:10.1029/2009JD011869

Chen YH, Del Genio AD (2009) Evolution of tropical cloud regimes in observations and a general circulation model. Clim Dyn 32:355–369. doi:10.1007/S00382-008-0386-6

Drbohlav H, Wang B (2005) Mechanism of the northward propagating intraseasonal oscillation: insights from a zonally symmetric model. J Clim 18:952–972. doi:10.1175/JCLI3306.1

Duchon CE (1979) Lanczos filtering in one and two dimensions. J Appl Meteorol 18:1016–1022

Fu X, Wang B, Li T, McCreary JP (2003) Coupling between northward-propagating, intraseasonal oscillations and sea surface temperature in the Indian Ocean. J Atmos Sci 60:1733–1753

Fu X, Wang B, Tao L (2006) Satellite data reveal the 3-D moisture structure of tropical intraseasonal oscillation and its coupling with underlying ocean. Geophys Res Lett 33:L03705. doi:10.1029/2005GL025074

Goswami BN (2005) South Asian summer monsoon. In: Lau WK-M, Waliser DE (eds) Intraseasonal variability of the atmosphere-ocean climate system. Springer, Berlin, pp 19–61

Goswami BN, Shukla J (1984) Quasi-periodic oscillations in a symmetric general circulation model. J Atmos Sci 41:20–37

Goswami BN, Xavier PK (2003) Potential predictability and extended range prediction of Indian summer monsoon breaks. Geophys Res Lett 30(18):1966. doi:10.1029/2003GL017,810,2003

Goswami BN, Wheeler MC, Gottschalck JC, Waliser DE (2011) Intra-seasonal variability and forecasting: a review of recent research. The global monsoon system: research and forecast, vol 5, 2nd edn. World Scientific Publication Company in collaboration with WMO, pp 389–407

Grecu M, Olson WS (2006) Bayesian estimation of precipitation from satellite passive microwave observations using combined radar–radiometer retrievals. J Appl Meteor Climatol 45:416–433

Grecu M, Olson WS, Shie C-L, L'Ecuyer TS, Tao W-K (2009) Combining satellite microwave radiometer and radar observations to estimate atmospheric latent heating profiles. J Clim 22:6356–6376

Haddad ZS, Smith EA, Kummerow CD, Iguchi T, Farrar MR, Durden SL, Alves M, Olson WS (1997a) The TRMM 'day-1' radar/radiometer combined rain-profiling algorithm. J Meteorol Soc Jpn 75:799–809

Haddad ZS, Short DA, Durden SL, Im E, Hensley S, Grable MB, Black RA (1997b) A new parametrization of the rain drop size distribution. IEEE Trans Geosci Remote Sens 35:532–539. doi:10.1109/36.581961

Houze RA (1997) Stratiform precipitation in regions of convection: a meteorological paradox? Bull Am Meteorol Soc 78:2179–2196

Houze RA (2004) Mesoscale convective systems. Rev Geophys 42:4. doi:10.1029/2004RG000150

Huffman GJ, Adler RF, Morrissey M, Bolvin DT, Curtis S, Joyce R, McGavock B, Susskind J (2001) Global precipitation at one-degree daily resolution from multi-satellite observations. J Hydrometeorol 2:36–50. doi:10.1175/1525-7541(2001)002<0036:GPAODD>2.0.CO;2

Huffman GJ, Adler RF, Bolvin DT, Gu G, Nelkin EJ, Bowman KP, Hong Y, Stocker EF, Wolff DB (2007) The TRMM multisatellite precipitation analysis (TMPA): quasi-global, multiyear, combined-sensor precipitation estimates at fine scales. J Hydrometeorol 8:38–55

Iguchi T, Kozu T, Meneghini R, Awaka J, Okamoto K (2000) Rain profiling algorithm for the TRMM precipitation radar. J Appl Meteorol 39:2038–2052

Jakob C, Tselioudis G (2003) Objective identification of cloud regimes in the tropical western Pacific. Geophys Res Lett 30:2082. doi:10.1029/2003GL018367

Jiang X, Li T, Wang B (2004) Structures and mechanisms of the northward propagating boreal summer intraseasonal oscillation. J Clim 17:1022–1039

Jiang X, Waliser DE, Li JL, Woods C (2011a) Vertical cloud structures of the boreal summer intraseasonal variability based on CloudSat observations and ERA-interim reanalysis. Clim Dyn 36:2219–2232. doi:10.1007/s00382-010-0853-8

Jiang X, Waliser DE, Olson WS, Tao W-K, L'Ecuyer TS, Shige S, Li K-F, Yung YL, Lang S, Takayabu YN (2011b) Vertical diabatic heating structure of the MJO: intercomparison between recent reanalyses and TRMM estimates. Mon Weather Rev 139:3208–3223

Kikuchi K, Takayabu YN (2004) The development of organized convection associated with the MJO during TOGA COARE IOP: trimodal characteristics. Geophys Res Lett 31:L10101. doi:10.1029/2004GL019601

Kummerow C, Barnes W, Kozu T, Shiue J, Simpson J (1998) The tropical rainfall measuring mission (TRMM) sensor package. J Atmos Oceanic Technol 15:809–817

Kummerow C, Simpson J, Thiele O, Barnes W, Chang ATC, Stocker E, Adler RF, Hou A, Kakar R, Wentz F, Ashcroft P, Kozu T, Hong Y, Okamoto K, Iguchi T, Kuroiwa H, Im E, Haddad Z, Huffman G, Ferrier B, Olson WS, Zipser E, Smith EA, Wilheit TT, North G, Krishnamurti TN, Nakamura K (2000) The status of the tropical rainfall measuring mission (TRMM) after 2 years in orbit. J Appl Meteorol 39:1965–1982

Kummerow C, Hong Y, Olson WS, Yang S, Adler RF, McCollum J, Ferraro R, Petty G, Shin DB, Wilheit TT (2001) The evolution of the Goddard profile algorithm (GPROF) for rainfall estimation from passive microwave sensors. J Appl Meteorol 40:1801–1820

Lau WKM, Waliser DE (2005) Intraseasonal variability in the atmosphere–ocean climate system. Springer, Heidelberg, p 474

Lawrence DM, Webster PJ (2002) The boreal summer intraseasonal oscillation: relationship between northward and eastward movement of convection. J Atmos Sci 59:1593–1606

Lin JL, Weickman KM, Kiladis GN, Mapes BE, Schubert SD, Suarez MJ, Bacmeister JT, Lee MI (2008) Subseasonal variability associated with Asian summer monsoon simulated by 14 IPCC AR4 coupled GCMs. J Clim 21:4541–4567. doi:10.1175/2008JCLI1816.1

Madden RA, Julian PR (1971) Detection of a 40–50 day oscillation in zonal wind in tropical Pacific. J Atmos Sci 28:702–708

Madden RA, Julian PR (1994) Observations of the 40–50-day tropical oscillation: a review. Mon Weather Rev 122:814–837

Prasanna V, Annamalai H (2012) Moist dynamics of extended monsoon breaks over south Asia. J Clim 25:3810–3831. doi:10.1175/JCLI-D-11-00459.1

Rossow WB, Tselioudis G, Polak A, Jakob C (2005) Tropical climate described as a distribution of weather states indicated by distinct mesoscale cloud property mixtures. Geophys Res Lett 32:L21812. doi:10.1029/2005GL024584

Sikka DR, Gadgil S (1980) On the maximum cloud zone and the ITCZ over Indian, longitudes during the southwest monsoon. Mon Weather Rev 108:1840–1853

Tian B, Waliser DE, Fetzer EJ, Lambrigtsen BH, Yung Y, Wang B (2006) Vertical moist thermodynamic structure and spatial-temporal evolution of the MJO in AIRS observations. J Atmos Sci 63:2462–2485

Tromeur E, Rossow WB (2010) Interaction of tropical deep convection with the large-scale circulation in the MJO. J Clim 23:1837–1853

Waliser DE (2006) Intraseasonal variations. In: Wang B (ed) The Asian monsoon. Springer, Heidelberg, p 787

Wang B, Xie X (1997) A model for the boreal summer intraseasonal oscillation. J Atmos Sci 54:72–86

Wang N-Y, Liu C, Ferraro R, Wolff D, Zipser E, Kummerow C (2009) The TRMM 2A12 land precipitation product-status and future plans. J Meteorol Soc Jpn 87A:237–253

Webster PJ (1983) Mechanisms of monsoon low-frequency variability: surface hydrological effects. J Atmos Sci 40:2110–2124

Webster PJ, Hoyos C (2004) Prediction of monsoon rainfall and river discharge on 15–30 day time scales. Bull Amer Met Soc 85(11):1745–1765

Wong S, Fetzer EJ, Tian B, Lambrigtsen B (2011) The apparent water vapor sinks and heat sources associated with the intraseasonal oscillation of the Indian summer monsoon. J Clim 24:4466–4479

Xavier PK, Marzin C, Goswami BN (2007) An objective definition of the Indian summer monsoon season and a new perspective on the ENSO-monsoon relationship. Quart J Roy Meteor Soc 133:749–764

Yang B, Fu X, Wang B (2008) Atmosphere-ocean conditions jointly guide convection of the boreal summer intraseasonal oscillation: satellite observations. J Geophys Res 113:D11105. doi:10.1029/2007JD009276

Zhang CD (2005) Madden-Julian oscillation. Rev Geophys 43:RG2003. doi:10.1029/2004RG000158

Zhang C, Ling J, Hagos SM, Tao W-K, Lang S, Takayabu YN, Shige S, Katsumata M, Olson WS, L'Ecuyer T (2010) MJO signals in latent heating: results from TRMM retrievals. J Atmos Sci 67:3488–3508